

Real-time counting of single electron tunneling through a T-shaped double quantum dot system

JunYan Luo,^{1,2,*} Shi-Kuan Wang,³ Xiao-Ling He,¹ Xin-Qi Li,^{2,3,4} and YiJing Yan^{2,†}

¹*School of Science, Zhejiang University of Science and Technology, Hangzhou 310023, China*

²*Department of Chemistry, Hong Kong University of Science and Technology, Kowloon, Hong Kong SAR, China*

³*State Key Laboratory for Superlattices and Microstructures, Institute of Semiconductors, Chinese Academy of Sciences, P.O. Box 912, Beijing 100083, China*

⁴*Department of Physics, Beijing Normal University, Beijing 100875, China*

(Dated: September 28, 2018)

Real-time detection of single electron tunneling through a T-shaped double quantum dot is simulated, based on a Monte Carlo scheme. The double dot is embedded in a dissipative environment, and the presence of electrons on the double dot is detected with a nearby quantum point contact. We demonstrate directly the bunching behavior in electron transport, which leads eventually to a super-Poissonian noise. Particularly, in the context of full counting statistics, we investigate the essential difference between the dephasing mechanisms induced by the quantum point contact detection and the coupling to the external phonon bath. A number of intriguing noise features associated with various transport mechanisms are revealed.

PACS numbers: 72.70.+m, 73.23.Hk, 73.63.-b, 03.65.Ta

I. INTRODUCTION

To control and manipulate electronic dynamics in nanoscale devices it requires knowledge of the involving transport processes at single-electron level. The spectrum of current fluctuations, which characterizes the degree of correlation between charge transport events, serves as an essential tool superior to the average current in distinguishing various transport mechanisms.^{1,2} Full counting statistics (FCS) of current^{3,4} has also been measured,^{5–10} owing in particular to the development of highly sensitive on-chip detection of single-electron tunneling technique. All statistical cumulants of the number of transferred particles can now be extracted experimentally.

Current fluctuations would obey a Poissonian process if the tunneling events were statistically independent. However, non-Poissonian fluctuation is in general a reality. In the case of transport through a localized state, the Pauli exclusion principle suppresses the noise,¹¹ leading to a sub-Poissonian statistics. Systems of multiple non-local states such as coupled quantum dots¹² are more interesting. The intrinsic quantum coherence and many-particle interactions there result in different sources of correlations. The fascinating super-Poissonian noise thus occurs in various contexts, and thereby has been attracting a wide interest recently.

A representing system, which will be studied in this work, is a T-shaped double quantum dot (TDQD) system,^{13–15} as schematically shown in Fig. 1. The system is of particular interest, as it can be mapped to a structure of quantum well in presence of an impurity inside, which has been investigated experimentally.¹⁶ The source and drain electrodes of the TDQD are in such a configuration that maximizes locality versus nonlocality contrast. In addition, the TDQD is also influenced by an inevitable dissipative environment. The nearby quantum

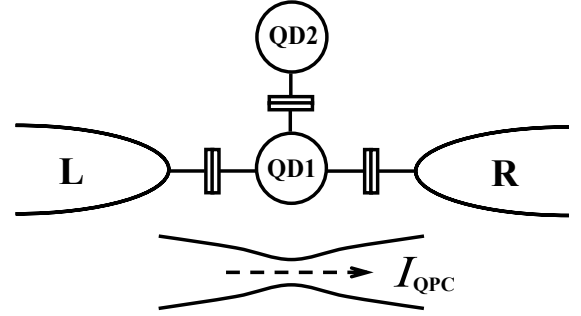


FIG. 1: Schematics of electron transport through a TDQD system, monitored continuously by the QPC current that depends on the charge state for excess electrons on two dots individually. The TDQD is also coupled to an inevitable dissipative phonon environment (not shown explicitly).

point contact (QPC) that serves as a charge detector is asymmetrically coupled to the dots. The current through the QPC depends on the charge state, (n_1, n_2) , for excess electrons on two dots individually. Electron tunneling through the TDQD results in temporal changes in the charge state, and thus fluctuations in the QPC current.

In this work, we first simulate the real-time detection of single electron tunneling through TDQD in experimental setup of Fig. 1. The real-time simulation will be carried out based on a Monte Carlo approach to quantum master equation.¹⁷ In particular, we demonstrate transparently the electron bunching, i.e., the super-Poissonian noise of charge transfer. The FCS is then studied, and the result shows good agreement with those obtained from Monte Carlo simulation. It therefore verifies the validity of our Monte Carlo method for real-time measurement. Particularly, it is found that the FCS is capable of differentiating between the dephasing effect induced by the

QPC charge detection and that by the coupling to the dissipative bath environment. A number of intriguing noise features will be revealed in association with various mechanisms, demonstrating thus the sensitivity and selectivity of cumulants to different transport properties.

The paper is organized as follows. We describe the TDQD system and conditional quantum master equation in Sec. II. The Monte Carlo simulation of real-time detection of single electron tunneling is summarized in Sec. III, together with the electron bunching behavior demonstrated vividly for the system in study. Having the FCS theory reviewed in Sec. IV, we present the results and discussions in Sec. V. Finally, we conclude in Sec. VI.

II. QUANTUM MASTER EQUATION THEORY OF QUANTUM MEASUREMENT

A. Model device

Let us start with the model setup for the QPC detection of single-electron tunneling through TDQD, as sketched in Fig. 1. The total Hamiltonian consists of the coupled dots system, the environment, and the coupling between them; i.e. $H = H_{\text{sys}} + H_{\text{env}} + H_{\text{sys-env}}$. The electron Hamiltonian for the coupled dots system reads

$$H_{\text{sys}} = \sum_{\sigma} \left(\frac{1}{2} \epsilon \hat{Q}_{z\sigma} + \Omega \hat{Q}_{x\sigma} \right) + \sum_l U_l \hat{n}_{l\uparrow} \hat{n}_{l\downarrow} + U' \hat{n}_1 \hat{n}_2, \quad (1)$$

where $\hat{Q}_{z\sigma} \equiv d_{1\sigma}^{\dagger} d_{1\sigma} - d_{2\sigma}^{\dagger} d_{2\sigma}$, $\hat{Q}_{x\sigma} \equiv d_{1\sigma}^{\dagger} d_{2\sigma} + d_{2\sigma}^{\dagger} d_{1\sigma}$, $\hat{n}_l = \sum_{\sigma} \hat{n}_{l\sigma}$, and $\hat{n}_{l\sigma} = d_{l\sigma}^{\dagger} d_{l\sigma}$, with $d_{l\sigma}$ ($d_{l\sigma}^{\dagger}$) the electron annihilation (creation) operator in the QD1 ($l = 1$) or QD2 ($l = 2$). Each quantum dot is assumed to have only one spin-degenerate level ($\sigma = \uparrow$ or \downarrow) in the bias window. The level detuning between the two dots is $\epsilon = \epsilon_1 - \epsilon_2$. The interdot coupling strength is Ω . The intradot and interdot Coulomb interactions, U_l and U' , are both assumed to be much larger than the Fermi levels. We shall be interested in the double-dot Coulomb blockade regime,^{18,19} i.e. at most one electron resides in the TDQD. It can be realized in experiments by proper tuning the gate and bias voltages.²⁰

The environment is of $H_{\text{env}} = h_{\text{ph}} + \sum_{\alpha} h_{\alpha} + h_{\text{QPC}}$. It is composed of the phonon bath, the electron reservoirs of the source and drain ($\alpha = \text{L}$ and R) electrodes, as well as the QPC detector. Each of them is modeled as a collection of noninteracting particles. The phonon bath assumes $h_{\text{ph}} = \frac{1}{2} \sum_j \hbar \omega_j (p_j^2 + x_j^2)$. The electron reservoirs are modeled with $h_{\alpha} = \sum_{k,\sigma} \epsilon_{\alpha k} c_{\alpha k \sigma}^{\dagger} c_{\alpha k \sigma}$ and $h_{\text{QPC}} = \sum_{p,\sigma} \epsilon_p c_{p\sigma}^{\dagger} c_{p\sigma} + \sum_{q,\sigma} \epsilon_q c_{q\sigma}^{\dagger} c_{q\sigma}$, respectively. These electronic parts are written in terms of electron creation and annihilation operators in the α -electrode and the QPC reservoirs states.

The system–environment coupling can be written as

$$H_{\text{sys-env}} = \sum_{\sigma} \hat{Q}_{z\sigma} F_{\text{ph}} + \sum_{\alpha,\sigma} (d_{1\sigma}^{\dagger} f_{\alpha\sigma} + f_{\alpha\sigma}^{\dagger} d_{1\sigma}) + \sum_{s=0,1,2} \hat{n}_s F_s^{\text{QPC}}. \quad (2)$$

The first term describes the coupling with phonon bath, in which $F_{\text{ph}} \equiv \sum_j \lambda_j x_j$. This term is responsible for the dot level energy fluctuations. The effect of phonon bath on the double-dot system is characterized by the phonon interaction spectral density, $J_{\text{ph}}(\omega) = \sum_j |\lambda_j|^2 \delta(\omega - \omega_j)$. The second term describes the transfer coupling between QD1 and the leads, in which $f_{\alpha\sigma} \equiv \sum_k t_{\alpha k \sigma} c_{\alpha k \sigma}$. The third term describes the interaction between the QPC detector and the measured system, in which $F_s^{\text{QPC}} \equiv \sum_{p,q,\sigma} (t_{spq} c_{p\sigma}^{\dagger} c_{q\sigma} + \text{H.c.})$. The amplitude of electron tunneling through the QPC depends on the TDQD charge state $\hat{n}_s = |s\rangle\langle s|$, with $s = 0$ for no excess electrons, and $s = 1$ or 2 for one excess electron in QD1 or QD2, respectively. In other words, the current through the QPC sensitively depends on the charge states of the TDQD, and thus can be used to measure single electron tunneling events. The effects of these electron reservoirs components on the double-dot system are characterized individually by their interaction spectral densities: $J_{\alpha}(\omega) = \sum_{k\sigma} |t_{\alpha k \sigma}|^2 \delta(\omega - \epsilon_{\alpha k})$, and $J_s^{\text{QPC}}(\omega) = \sum_{p,q,\sigma} |t_{spq}|^2 \delta(\omega - \epsilon_{p\sigma} + \epsilon_{q\sigma})$, respectively.

In the Coulomb blockade regime, together with large source–drain voltage, the tunneling between QD1 and the electrode $\alpha = \text{L}$ or R can be characterized by the rate $\Gamma_{\alpha}(\omega) = 2\pi \sum_{k\sigma} |t_{\alpha k \sigma}|^2 \delta(\omega - \epsilon_{\alpha k})$. In what follows we adopt flat bands in the electrodes, which yields energy independent couplings Γ_{α} . Analogously, the coupling with the QPC is described by the rate $\mathcal{T}_s = 2\pi g_p g_q |t_{spq}|^2 V_{\text{QPC}}$, where V_{QPC} is the QPC bias voltage, g_p and g_q are the density of states in the QPC reservoirs. We assume hereafter the density of states to be constant, and t_{spq} reservoir states independent. Thus \mathcal{T}_s just depends on the system charge occupation state $|s\rangle\langle s|$, with $s = 0$ being for zero excess electron, and $s = 1$ or 2 for one excess electron in QD1 or QD2, respectively. For the QPC current, $I_s = e\mathcal{T}_s$, we have $I_0 > I_2 > I_1$, as implied in the scheme of Fig. 1.

B. Quantum master equation theory

To describe the quantum measurement, we exploit the reduced density operator $\rho^{(n)}(t)$ of the TDQD system, for the specified number n electrons having passed through the QPC detector and being recorded up to the given time. The related conditional quantum master equation can be derived, which is greatly simplified under the Born–Markov approximation.^{18,19,21,22} Here, instead of using the “ n ”-resolved equation directly, it is convenient to introduce its χ -space counterpart via $\rho(\chi, t) \equiv \sum_n e^{in\chi} \rho^{(n)}(t)$, where χ is the so-called count-

ing field. Let the quantum master equation be formally

$$\frac{\partial}{\partial t}\rho(\chi, t) = -(i\mathcal{L} + \mathcal{R}_\chi)\rho(\chi, t), \quad (3)$$

where $\mathcal{L} \cdot \equiv [H_{\text{sys}}, \cdot]$ is the system Liouvillian, and \mathcal{R}_χ is the dissipation superoperator to be specified soon. Hereafter, we set unit of $\hbar = e = 1$ for the Planck constant and electron charge, unless where is needed for clarity.

To that end, let us recast the reduced density matrix in the vector notation,

$$\rho = (\rho_{00}, \rho_{11}, \rho_{22}, \rho_{12}, \rho_{21}, \rho_{1\bar{1}}, \rho_{2\bar{2}}, \rho_{1\bar{2}}, \rho_{2\bar{1}})^T, \quad (4)$$

with $\rho_{ss'} \equiv \langle s \uparrow | \rho | s \uparrow \rangle$ and $\rho_{s\bar{s}'} \equiv \langle s \downarrow | \rho | s \downarrow \rangle$. There

are 9 nonzero elements of the reduced density matrix in the Coulomb blockade regime. The other 16 elements, describing coherence between different spin states, are all zeroes as the system–environment coupling consider here does not cause spin flip. The dissipation superoperator \mathcal{R}_χ in Eq. (3) is simply a 9×9 matrix.

In the large voltage limit and Coulomb blockade regime, the involving Fermi functions can be approximated by the step function of either one or zero. Under the Born-Markov approximation for weak tunnel coupling and second-order perturbation theory in the electron–phonon coupling, the dissipation superoperator \mathcal{R}_χ matrix is obtained explicitly

$$\mathcal{R}_\chi = \begin{pmatrix} 2\Gamma_L + \mathcal{T}_0 q(\chi) & -\Gamma_R & 0 & 0 & 0 & -\Gamma_R & 0 & 0 & 0 \\ -\Gamma_L & \Gamma_R + \mathcal{T}_1 q(\chi) & 0 & 0 & 0 & 0 & 0 & 0 & 0 \\ 0 & 0 & \mathcal{T}_2 q(\chi) & 0 & 0 & 0 & 0 & 0 & 0 \\ 0 & \Gamma_+ & \Gamma_- & \Gamma_d & 0 & 0 & 0 & 0 & 0 \\ 0 & \Gamma_+ & \Gamma_- & 0 & \Gamma_d & 0 & 0 & 0 & 0 \\ -\Gamma_L & 0 & 0 & 0 & 0 & \Gamma_R + \mathcal{T}_1 q(\chi) & 0 & 0 & 0 \\ 0 & 0 & 0 & 0 & 0 & 0 & \mathcal{T}_2 q(\chi) & 0 & 0 \\ 0 & 0 & 0 & 0 & 0 & 0 & \Gamma_+ & \Gamma_- & \Gamma_d & 0 \\ 0 & 0 & 0 & 0 & 0 & 0 & \Gamma_+ & \Gamma_- & 0 & \Gamma_d \end{pmatrix}. \quad (5)$$

Here we have introduced

$$\Gamma_\pm = \frac{\pi}{2} \frac{\Omega}{\Delta} J_{\text{ph}}(\Delta) \left[1 \pm \frac{\epsilon}{\Delta} \coth\left(\frac{\Delta}{2k_B T}\right) \right], \quad (6)$$

$$\Gamma_d = \frac{1}{2}(\Gamma_R + \gamma_{\text{ph}} + \gamma_\chi), \quad (7)$$

and

$$\gamma_{\text{ph}} = 2\pi \frac{\Omega^2}{\Delta^2} J_{\text{ph}}(\Delta) \coth\left(\frac{\Delta}{2k_B T}\right), \quad (8)$$

$$\gamma_\chi = (\sqrt{\mathcal{T}_1} - \sqrt{\mathcal{T}_2})^2 + 2\sqrt{\mathcal{T}_1 \mathcal{T}_2} q(\chi), \quad (9)$$

with $q(\chi) \equiv 1 - e^{i\chi}$, $\Delta \equiv \sqrt{\epsilon^2 + 4\Omega^2}$ the Rabi frequency of the double-dot system, k_B the Boltzman constant, and T the temperature. The physical processes described by the transfer elements in Eq. (5) are clear.^{23–25}

Consider $\mathcal{R}_{11,00}^\chi = -\Gamma_L$, $\mathcal{R}_{00,11}^\chi = -\Gamma_R$, and their opposite spin counterparts, as inferred from Eq. (5). These identities agree with the sequential tunneling picture, with Γ_L being the rate of electron tunneling from the left electrode to system, and Γ_R being that from system to the right electrode; both via QD1.

The parameter Γ_\pm [Eq. (6)] denotes the nonsecular elements for the population–to–coherence transfers: $\Gamma_+ \equiv$

$\mathcal{R}_{12,11}^\chi = \mathcal{R}_{21,11}^\chi$, $\Gamma_- \equiv \mathcal{R}_{12,22}^\chi = \mathcal{R}_{21,22}^\chi$, and their opposite spin counterparts, as denoted in Eq. (5). They are purely due to the phonon bath environment.

The parameter Γ_d [Eq. (7)] is the total decoherence rate between two levels: $\Gamma_d \equiv \mathcal{R}_{12,12}^\chi = \mathcal{R}_{21,21}^\chi$ and the opposite spin counterparts, as denoted in Eq. (5). The total decoherence rate is composed of not just Γ_R due to the electron depopulation to collector, but also γ_{ph} [Eq. (8)] and γ_χ [Eq. (9)], due to the phonon bath coupling and the QPC detection, respectively. Note that $\gamma_d \equiv \gamma_{\chi=0} = (\sqrt{\mathcal{T}_1} - \sqrt{\mathcal{T}_2})^2$ denotes the dephasing rate induced by the existence of QPC ensemble.

In the numerical demonstrations below, we set the phonon bath spectral density $J_{\text{ph}}(\omega) = 2\eta\omega e^{-\omega/\omega_c}$. Here, the dimensionless parameter η reflects the strength of dissipation and ω_c is the Ohmic high energy cutoff.

III. MONTE CARLO SIMULATION OF SINGLE ELECTRON TUNNELING

Experimentally, the most intuitive method for measuring the FCS of electron transport is to count electrons passing one by one through the conductor. The real-time detection of single electron transport enables direct evaluation of the probability distribution function of the number of electrons transferred through device within a given time period. In addition to the current and the

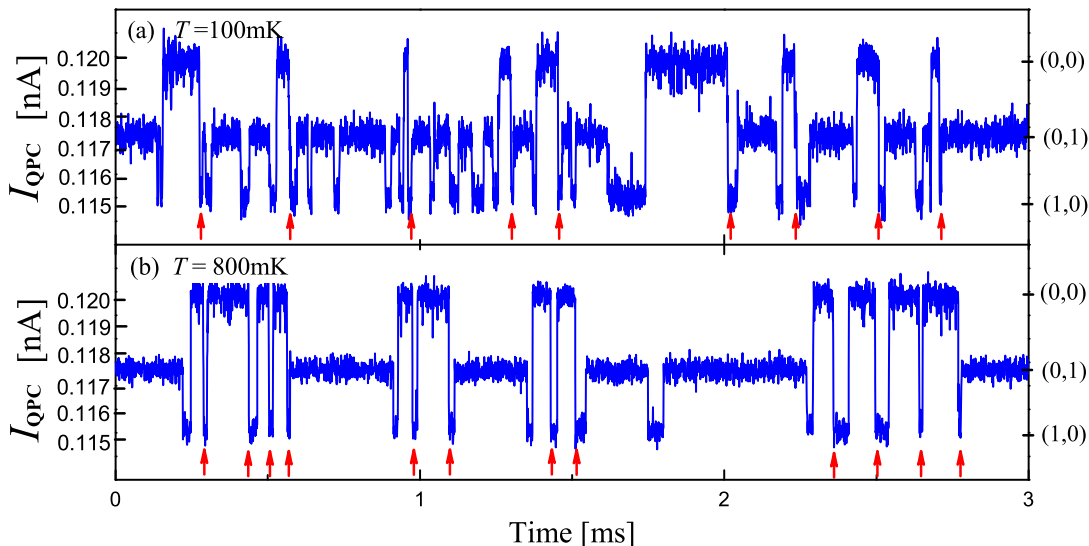


FIG. 2: Time traces of the QPC current fluctuations correspond to different charge states in the TDQD (shown on the right). The arrows indicate transitions where an electron is entering the QD1 from the left lead. (a) and (b) correspond to different temperatures $T = 100$ mK and $T = 800$ mK, respectively. Other parameters are: $\Gamma_R = 4\Gamma_L = \Omega = 20$ kHz, $\epsilon = -4\Omega$, $\eta = 2 \times 10^{-6}$, and $\omega_c = 0.4$ meV. The time step used is $\tau = 0.002$ ms, such that the minimum characteristic time-scale of the system can be clearly resolved.

shot noise, which are the first and second moments of this distribution, this method gives also access to higher order cumulants.

Here we outline the Monte Carlo simulation scheme for single electron tunneling through device.¹⁷ Let us start with the quantum master equation (3) and denote $\mathcal{L}_\chi \equiv -i\mathcal{L} - \mathcal{R}_\chi$ there. The solution to the reduced state simply reads $\rho(\chi, t) = e^{\mathcal{L}_\chi \delta t} \rho(\chi, t_0)$, for an arbitrary initial condition $\rho(\chi, t_0) = \rho(t_0)$ and finite time interval $\delta t \equiv t - t_0$. Its counterpart in the particle number “ n ”-space is obtained via the inverse Fourier transform

$$\rho^{(n)}(t) = \int_0^{2\pi} \frac{d\chi}{2\pi} e^{\mathcal{L}_\chi \delta t - in\chi} \rho(t_0) \equiv \mathcal{U}(n, \delta t) \rho(t_0). \quad (10)$$

The involving propagator $\mathcal{U}(n, \delta t)$ is completely determined by the dynamic structure of the master equation (3), regardless of the initial state. Therefore, we can numerically evaluate it by a “one-time task”, such as fast Fourier transform, which results in an efficient real-time simulation.

Specifically, consider the evolution of state $\rho(t_j)$ at t_j to $\rho^{(n_j)}(t_j + \tau)$ at $t_j + \tau$: $\rho^{(n_j)}(t_j + \tau) = \mathcal{U}(n_j, \tau) \rho(t_j)$, and denote $\text{Pr}(n_j) \equiv \text{Tr}[\rho^{(n_j)}(t_j + \tau)]$ that is the probability of having n_j electrons passed through QPC during the time interval $[t_j, t_j + \tau]$. If the measurement is made but the result is ignored, then the (mixture) state reads

$$\rho(t_j + \tau) = \sum_{n_j} \rho^{(n_j)}(t_j + \tau) = \sum_{n_j} \text{Pr}(n_j) \rho^c(n_j, t_j + \tau). \quad (11)$$

Here, $\rho^c(n_j, t_j + \tau) = \rho^{(n_j)}(t_j + \tau) / \text{Pr}(n_j)$ is the normalized state, conditioned by the definite number of n_j

electrons having passed through QPC during $[t_j, t_j + \tau]$. The second equality of Eq. (11) implies that if we stochastically generate n_j according to $\text{Pr}(n_j)$ for each time interval $[t_j, t_j + \tau]$, and collapse the state definitely onto $\rho^c(n_j, t_j + \tau)$, we have in fact simulated a particular realization for the selective state evolution conditioned on the specific measurement results.

For the output current in a particular real-time measurement, we have

$$I_{\text{QPC}}(t) = I_0 \rho_{00}^c + I_1 (\rho_{11}^c + \rho_{\bar{1}\bar{1}}^c) + I_2 (\rho_{22}^c + \rho_{\bar{2}\bar{2}}^c) + \xi(t). \quad (12)$$

The first three terms determine the conditional evolution of the charge state. The last term $\xi(t)$ originates from the intrinsic noise of detector. Here, we consider in the diffusive regime, where $\xi(t)$ is a Gaussian variable with zero mean value and the spectral density $S_\xi = 2e \langle I_{\text{QPC}} \rangle$, with $\langle I_{\text{QPC}} \rangle$ the average stationary QPC current. Accordingly, we can stochastically generate n_j , the number of electrons having passed through QPC during $[t_j, t_j + \tau]$, via $n_j = \int_{t_j}^{t_j + \tau} dt' I_{\text{QPC}}(t') = [I_0 \rho_{00}^c + I_1 (\rho_{11}^c + \rho_{\bar{1}\bar{1}}^c) + I_2 (\rho_{22}^c + \rho_{\bar{2}\bar{2}}^c)] \tau + dW(t_j)$, where $dW(t_j)$ is the Wiener increment during $[t_j, t_j + \tau]$.

A typical example of simulated real-time detector current I_{QPC} is displayed in Fig. 2 for (a) $T = 100$ mK and (b) $T = 800$ mK, respectively. The temperatures are much smaller than the bias voltage across the TDQD, as well as the interdot and the intradot charging energies. Thus, electrons are transported in one direction, i.e. from the left lead to the right one. The corresponding charge states (n_1, n_2) of the TDQD, with n_1 and n_2 being the excess electrons in QD1 and QD2, respectively, are shown

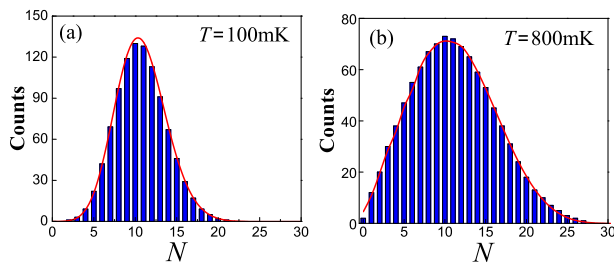


FIG. 3: Statistical distribution of the number N of electrons entering the TDQD during a given measurement time span of $t_c = 3$ ms for (a) $T = 100$ mK, and (b) $T = 800$ mK, respectively. The other parameters are the same as in Fig. 2. The solid line shows the distribution calculated from Eq. (16).

on the right. We choose rates of tunneling to the left and right leads as $\Gamma_L = 5$ kHz and $\Gamma_R = 20$ kHz, such that all the tunneling rates are within the bandwidth (~ 30 kHz) of the QPC detector.⁹ The QPC conductance (without excess electrons in TDQD) is $G_0 = 0.02 e^2/h$, and QPC bias voltage $V_{\text{QPC}} = 0.15$ mV, which corresponds to a QPC current $I_0 \approx 0.12$ nA. The conductance is assumed to decrease by 4% or 2%, when an electron occupies on the QD1 or QD2, respectively. The corresponding QPC currents are $I_1 \approx 0.115$ nA and $I_2 \approx 0.118$ nA. The rate of dephasing due to QPC charge detection²⁶ is then determined as $\gamma_d = \frac{1}{e}(\sqrt{I_1} - \sqrt{I_2})^2 \approx 75$ kHz.

In Fig. 2, each arrow indicates the tunneling of one electron from the left lead into QD1. Accordingly, a charge state transition $(0,0) \rightarrow (1,0)$ occurs. Remarkably, we observe a clear signature of electron bunching, especially when temperature is high, as shown in Fig. 2(b). This phenomenon can be understood in terms of dynamical channel blockade, as will be explained later in more detail. For a thorough analysis of the statistical properties for electron transport through the TDQD device, we resort to the FCS. It is enabled by the probability distribution for the number N of electrons entering the QD1 from the left lead (the down steps indicated by arrows in Fig. 2) during a given time span t_c , by counting the number of electrons from the time traces analogous to the ones shown in Fig. 2. The obtained current distributions for $T = 100$ mK and $T = 800$ mK are displayed by histograms in Fig. 3(a) and (b), respectively, by repeating this counting procedure on one thousand independent traces with the measurement time span of $t_c = 3$ ms.

IV. FULL COUNTING STATISTICS THEORY

We consider hereafter the counting statistics of current through the TDQD device. The central quantity is then the probability that a given N electrons have passed through the device during the counting measurement time span t_c . This probability is related to the particle-number-resolved reduced density operator as

$P(N, t_c) \equiv \text{Tr} \rho^{(N)}(t_c)$, where the trace is over the system degrees of freedom. Note here “ N ” denotes the number of electrons transferred through the device, rather than the QPC detector considered earlier. From the knowledge of these probabilities one can easily derive not only the current and noise, but all the cumulants of the current distribution. The associated cumulant generating function (CGF) $g(\varphi)$ reads

$$e^{g(\varphi)} = \sum_N P(N, t_c) e^{-iN\varphi}, \quad (13)$$

where φ is the counting field on a specified TDQD lead. All cumulants of the current can be obtained from the CGF by performing derivatives with respect to the counting field

$$\langle I^k \rangle = -(-i\partial_\varphi)^k g(\varphi)|_{\varphi=0}. \quad (14)$$

The first three cumulants are related to the average current, the (zero-frequency) current noise, and the skewness, respectively.

To evaluate the CGF, let us consider $\varrho(\varphi, t) \equiv \sum_N \rho^{(N)}(t) e^{iN\varphi}$. Its equation of motion reads

$$\dot{\varrho}(\varphi, t) \equiv \mathcal{L}_\varphi \varrho(\varphi, t). \quad (15)$$

The involving generator \mathcal{L}_φ is completely determined by the associated conditional master equation,¹⁷ which is similar to Eq. (3) but with the number of electrons passing through the TDQD device being resolved. The formal solution to Eq. (15) is $\varrho(\varphi, t) = e^{\mathcal{L}_\varphi t} \varrho(\varphi, 0)$. Straightforwardly, the CGF is determined as $g(\varphi) = -\ln\{\text{Tr} \varrho(\varphi, t_c)\}$. Actually, we are most interested in the zero-frequency limit, i.e. the counting time t_c is much longer than the time of tunneling through the system. The CGF then simplifies to $g(\varphi) = -\lambda_{\min}(\varphi) t_c$, where $\lambda_{\min}(\varphi)$ is the minimal eigenvalue of \mathcal{L}_φ that satisfies $\lambda_{\min}(\varphi \rightarrow 0) \rightarrow 0$.^{4,27-29} With the knowledge of CGF, the distribution function can be readily obtained via³

$$P(N) = \int_0^{2\pi} \frac{d\varphi}{2\pi} e^{-g(\varphi) - iN\varphi}. \quad (16)$$

V. RESULTS AND DISCUSSIONS

In what follows, we focus our analysis on electron tunneling from the left lead to QD1. The relevant N is then the number of electrons entering the dot from left lead, and φ is the corresponding counting field. Note the same calculations apply to the counting for the right lead. The numerical results for the probability distribution are plotted by the solid lines in Fig. 3. It shows a striking agreement with the histograms obtained by Monte Carlo simulation; thus, it also verifies the validity of our Monte Carlo method for real-time measurement. The two distributions in Fig. 3(a) and (b) are rather different. The latter shows a broader and more asymmetric distribution

than the former. We characterize the differences quantitatively based on the FCS analysis, as follows.

Consider first the situation without electron-phonon interaction ($\eta = 0$). The first current cumulant gives the average current $\langle I \rangle = 2\Gamma_L\Gamma_R/\Gamma_{\text{eff}}$, with $\Gamma_{\text{eff}} \equiv 4\Gamma_L + \Gamma_R$ the total effective tunneling width.^{18,19} It is independent of level detuning ϵ , interdot coupling Ω , and QPC charge detection induced dephasing γ_d . In contrast to the current, valuable information can be extracted in the second cumulant (zero-frequency shot noise). By expressing it in terms of the Fano factor $F \equiv \langle I^2 \rangle / \langle I \rangle$, we readily obtain

$$F = 1 - \frac{8\Gamma_L\Gamma_R}{\Gamma_{\text{eff}}^2} + 2\Gamma_L^2\Gamma_R \frac{(\gamma_d + \Gamma_R)^2 + 4\epsilon^2}{(\gamma_d + \Gamma_R)\Gamma_{\text{eff}}^2\Omega^2}. \quad (17)$$

It thus allows us to get more knowledge than the current on the processes involved in the electronic transport. In Fig. 4(a), the Fano factor F is plotted against the level detuning ϵ for different QPC-induced dephasing rates γ_d .

Noticeably, a significantly enhanced Fano factor is expected when the dot levels are far from resonance. In this case, electron transitions between the two dots are suppressed. For instance, if an electron is tunneled into QD2, it will dwell on it for a long time. In the strong Coulomb blockade regime, the electron in QD2 will block the current until it is removed and tunneled out to the right lead. Consequently, a mechanism of dynamical channel blockade is developed,^{19,24,33–37} and the system exhibits strong electron bunching behavior, which leads eventually to a profound super-Poissonian noise.

It is worth noting that a strong super-Poissonian noise is more readily achieved for a small Ω [cf. Eq. (17)]. In this case, electron tunneling between the two dots is suppressed, which would enhance electron localization of electron in QD2. Electrons thus tend to be transferred in bunches. Remarkably, as $\Omega \rightarrow 0$ a diverging Fano factor is found. Here, the strong bunching behavior is responsible for the divergency.³⁸ Similar results were also reported in Ref. 39, where counting statistics for electron transport through a double-dot Aharonov-Bohm interferometer was investigated. However, in that case the divergence is closely related to a separation of the Hilbert space of the double-dot into disconnected subspaces that contain the spin singlet and triplet states for double occupancy.

The QPC charge detection has a two-fold effect on the measured system. On one hand, it causes dephasing between the two dot-levels. Generally, the dephasing mechanism leads to the suppression of noise,²⁴ which explains the γ_d -dependence of the Fano factor shown in Fig. 4, i.e. the noise is reduced with rising dephasing rate, particularly in the regime far from resonance. On the other hand, the measurement gives rise to the so-called quantum “Zeno” effect,^{30–32} which dominates in the regime of large dephasing rate, and results in a strong dynamic charge blockade behavior. The noise is finally enhanced with increasing dephasing rate, as we have checked (not shown in Fig. 4).

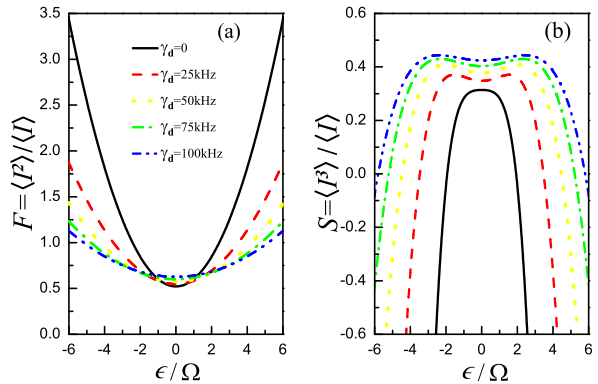


FIG. 4: (a) Fano factor and (b) normalized skewness versus level detuning for different QPC-induced dephasing rates. The electron charge is set to be $e = 1$. The temperature is $T = 100\text{mK}$, and the other parameters are the same as in Fig. 2, but in the absence of phonon bath; i.e., $\eta = 0$.

The Fano factor studied so far proves to be much sensitive than the average current, it only reveals, however, limited information about the QPC charge detection induced dephasing mechanism. We thus expect more information to be extracted in the next order cumulant, i.e. the skewness. The numerical results for the normalized skewness $S \equiv \langle I^3 \rangle / \langle I \rangle$ is displayed in Fig. 4(b) as a function of level detuning ϵ . Without QPC charge detection induced dephasing, the skewness reaches the maximum when the dot levels are in resonance ($\epsilon = 0$). As the dephasing rate grows, it turns into a local minimum. At the edges of the resonance a double maximum structure symmetric around $\epsilon = 0$ is observed. The local maxima shift away from resonance with increasing dephasing rates, as clearly demonstrated in Fig. 4(b).

Now let us turn to the influence of phonon heat bath that induces dephasing between two dots. We will reveal the essential difference between the dephasing induced via QPC charge detection and that by phonon coupling. The former can be modified via the coupling between the TDQD and the QPC, while the latter is generated with emission and absorption of phonons and increases with rising temperature. Here, we limit our discussions to the temperatures well below the Coulomb charging energies and the bias voltage. Therefore the temperature acts solely due to the coupling to the phonon heat bath.

The calculated Fano factor and normalized skewness versus level detuning are plotted in Fig. 5 for different temperatures. Increasing temperature results in the enhancement of phonon-bath induced dephasing, as the emission and absorption of phonons occur more frequently. Analogous to the QPC detection, it gives rise to a mechanism of localization in QD2, and consequently to a dynamical channel blockade. Eventually, electron transport through QD1 occurs in bunches during lapses of time when the QD2 is empty. This is confirmed by the real-time trajectory [cf. Fig. 2(b)]. Thus the noise in-

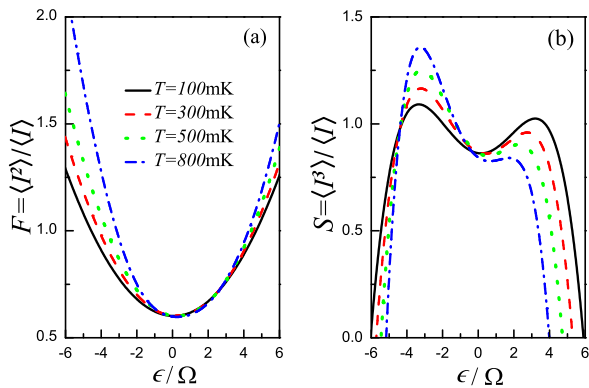


FIG. 5: (a) Fano factor and (b) normalized skewness versus level detuning for different temperatures with $\gamma_d = 75$ kHz. The electron charge is set to be $e = 1$. The other parameters are the same as in Fig. 2, including those of phonon heat bath of $\eta = 2 \times 10^{-6}$ and $\omega_c = 0.4$ meV.

creases with rising temperature, as displayed in Fig. 5(a).

If the TDQD is coupled only to the QPC, the cumulants are symmetric around $\epsilon = 0$, as shown in Fig. 4. However, with non-zero coupling to the heat bath the noise exhibits a clear asymmetry (see Fig. 5). This is essentially due to another consequences of phonon coupling: The phonon mediated transition can partially resolve the dynamical charge blockade.^{24,40} For instance, at zero temperature and $\epsilon > 0$, spontaneous phonon emission can partially lift the localization caused by dephasing, and the spectrum turns out to be asymmetric. Similar argument applies to the regime of finite temperature, where both phonon absorption and emission take place. The fact that emission is more likely than absorption explains the observed asymmetry.

The skewness of the current distribution, which was not explored in Ref. 24, is found to be more sensitive to thermal phonon bath-induced dephasing. Without coupling to the phonon bath, the skewness shows a symmetric double maximum structure. The spectral becomes asymmetric in the presence of electron-phonon interaction. With increasing temperature, the phonon absorption takes place more frequently at $\epsilon < 0$, and thus

greatly enhance the local maximum. While in the opposite regime of $\epsilon > 0$ the local maximum is reduced due to suppressed phonon emission.

VI. SUMMARY

We have investigated electron transport through a T-shaped double quantum dot system by utilizing a quantum master equation approach. The major advantage of the present approach is its simplicity of treating properly the dephasing mechanism of the QPC charge detection and that due to an external heat bath. In addition, this approach has the merit of dealing with other sources of dephasing, such as that entailed by anti-resonances.⁴¹ Particularly, based on the Monte Carlo scheme, real-time detection of single electron tunneling is simulated by exploiting the sensitivity of a current, passing through a nearby quantum point contact, to the fluctuating charge on the quantum dots. Owing to the interplay between the Coulomb interactions and the dephasing mechanisms, a strong bunching behavior in the charge transfer was detected, which leads eventually to a super-Poissonian noise.

Furthermore, full counting statistics of the transport current is analyzed based on the probability distribution, which is determined by ensemble average over a large number of single trajectories. It is demonstrated that the dephasing mechanism of the QPC charge detection and that owing to the external heat bath give rise to distinct and intriguing features. It thereby enables us to achieve a clear identification of different dephasing sources. Investigations of various processes involved in the electronic transport through similar devices are highly desirable in experiments.

Acknowledgments

Support from the National Natural Science Foundation of China under Grants No. 10904128, and the Research Grants Council of the Hong Kong Government (Grant No. 604709) are gratefully acknowledged.

* Electronic address: jylo@zust.edu.cn

† Electronic address: yyan@ust.hk

¹ Y. M. Blanter and M. Büttiker, Phys. Rep. **336**, 1 (2000).
² Y. V. Nazarov, *Quantum Noise in Mesoscopic Physics* (Kluwer, Dordrecht, 2003).
³ L. S. Levitov, H. W. Lee, and G. B. Lesovik, J. Math. Phys. **37**, 4845 (1996).
⁴ D. A. Bagrets and Y. V. Nazarov, Phys. Rev. B **67**, 085316 (2003).
⁵ W. Lu, Z. Ji, L. Pfeiffer, K. W. West, and A. J. Rimberg, Nature **423**, 422 (2003).
⁶ J. Bylander, T. Duty, and P. Delsing, Nature **434**, 361

(2005).

⁷ R. Schleser, E. Ruh, T. Ihn, K. Ensslin, D. C. Driscoll, and A. C. Gossard, Appl. Phys. Lett. **85**, 2005 (2004).
⁸ L. M. K. Vandersypen, J. M. Elzerman, R. N. Schouten, L. H. W. van Beveren, R. Hanson, and L. P. Kouwenhoven, Appl. Phys. Lett. **85**, 4394 (2004).
⁹ S. Gustavsson, R. Leturcq, B. Simovic, R. Schleser, T. Ihn, P. Studerus, K. Ensslin, D. C. Driscoll, and A. C. Gossard, Phys. Rev. Lett. **96**, 076605 (2006).
¹⁰ T. Fujisawa, T. Hayashi, R. Tomita, and Y. Hirayama, Science **312**, 1634 (2006).
¹¹ L. Y. Chen and C. S. Ting, Phys. Rev. B **43**, 4534 (1991).

- ¹² W. G. van der Wiel, S. D. Franceschi, J. M. Elzerman, T. Fujisawa, S. Tarucha, and L. P. Kouwenhoven, *Rev. Mod. Phys.* **75**, 1 (2003).
- ¹³ T.-S. Kim and S. Hershfield, *Phys. Rev. B* **63**, 245326 (2001).
- ¹⁴ P. S. Cornaglia and D. R. Grempel, *Phys. Rev. B* **71**, 075305 (2005).
- ¹⁵ I. Djuric, B. Dong, and H. L. Cui, *Appl. Phys. Lett.* **87**, 032105 (2005).
- ¹⁶ A. Nauen, I. Hapke-Wurst, F. Hohls, U. Zeitler, R. J. Haug, and K. Pierz, *Phys. Rev. B* **66**, 161303 (2002).
- ¹⁷ S.-K. Wang, J. S. Jin, and X.-Q. Li, *Phys. Rev. B* **75**, 155304 (2007).
- ¹⁸ J. Y. Luo, X.-Q. Li, and Y. J. Yan, *Phys. Rev. B* **76**, 085325 (2007).
- ¹⁹ J. Y. Luo, X.-Q. Li, and Y. J. Yan, *J. Phys.: Cond. Matt.* **20**, 345215 (2008).
- ²⁰ K. Ono, D. G. Austing, Y. Tokura, and S. Tarucha, *Science* **297**, 1313 (2002).
- ²¹ X. Q. Li, P. Cui, and Y. J. Yan, *Phys. Rev. Lett.* **94**, 066803 (2005).
- ²² X. Q. Li, J. Y. Luo, Y. G. Yang, P. Cui, and Y. J. Yan, *Phys. Rev. B* **71**, 205304 (2005).
- ²³ T. Brandes, *Phys. Rep.* **408**, 315 (2005).
- ²⁴ G. Kießlich, E. Schöll, T. Brandes, F. Hohls, and R. J. Haug, *Phys. Rev. Lett.* **99**, 206602 (2007).
- ²⁵ R. Aguado and T. Brandes, *Phys. Rev. Lett.* **92**, 206601 (2004).
- ²⁶ S. A. Gurvitz, *Phys. Rev. B* **56**, 15215 (1997).
- ²⁷ C. W. Groth, B. Michaelis, and C. W. J. Beenakker, *Phys. Rev. B* **74**, 125315 (2006).
- ²⁸ C. Flindt, T. Novotny, and A.-P. Jauho, *Europhys. Lett.* **69**, 475 (2005).
- ²⁹ G. Kießlich, P. Samuelsson, A. Wacker, and E. Schöll, *Phys. Rev. B* **73**, 033312 (2006).
- ³⁰ A. N. Korotkov and D. V. Averin, *Phys. Rev. B* **64**, 165310 (2001).
- ³¹ S. A. Gurvitz, L. Fedichkin, D. Mozyrsky, and G. P. Berman, *Phys. Rev. Lett.* **91**, 066801 (2003).
- ³² J. Y. Luo, H. J. Jiao, F. Li, X.-Q. Li, and Y. J. Yan, *J. Phys.: Cond. Matt.* **21**, 385801 (2009).
- ³³ A. Cottet, W. Belzig, and C. Bruder, *Phys. Rev. Lett.* **92**, 206801 (2004).
- ³⁴ M. Gattobigio, G. Iannaccone, and M. Macucci, *Phys. Rev. B* **65**, 115337 (2002).
- ³⁵ R. Sánchez, G. Platero, and T. Brandes, *Phys. Rev. Lett.* **98**, 146805 (2007).
- ³⁶ G. Kießlich, H. Sprekeler, and E. Schöll, *Semicond. Sci. Technol.* **19**, S37 (2004).
- ³⁷ A. Cottet and W. Belzig, *Europhys. Lett.* **66**, 405 (2004).
- ³⁸ F. Li, H. J. Jiao, J. Y. Luo, X.-Q. Li, and S. A. Gurvitz, *Physica E* **41**, 1707 (2009).
- ³⁹ D. Urban and J. König, *Phys. Rev. B* **79**, 165319 (2009).
- ⁴⁰ A. Braggio, C. Flindt, and T. Novotný, *J. Stat. Mech.: Theory Exp.* **2009**, P01048.
- ⁴¹ L. E. F. F. Torres, H. M. Pastawski, and E. Medina, *Europhys. Lett.* **73**, 164 (2006).